Nanoscale

Accepted Manuscript

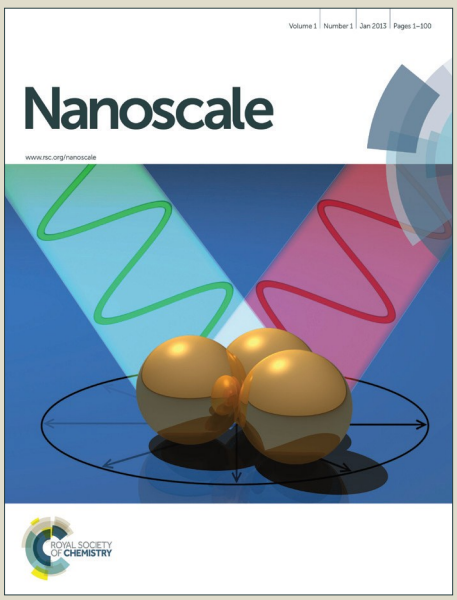

ROYAL SOCIETY OF CHEMISTRY

www.rsc.org/nanoscale

Nanoscale

COMMUNICATION

Ultraporous Nanocrystalline TiO_2-based Films: Synthesis, Patterning and Application as Anti-Reflective, Self-Cleaning, Superhydrophilic Coatings

Received 00th January 20xx,
Accepted 00th January 20xx

DOI: 10.1039/x0xx00000x

www.rsc.org/

M. Faustini,[a] A. Grenier [a], G. Naudin [a], Ronghua Li[a] and D. Grosso[a,b*]

Crack-free, anatase-based optical coatings with refractive index down to 1.27, porosity up to 80% vol, and tunable thickness up to 1.5 µm were fabricated. The extraordinary stability of the porosity upon thermal induced crystallisation and template removal was attributed to combined effects of the presence of 10% molar silica in the inorganic phase, a flash treatment at 500°C, and the use of templates with different dimensions ranging from a few nanometers to 50 nm. The hierarchical porous system was directely patterned by UV lithography and used as multifunctional anti-reflective, self-cleaning coatings.

Due to its natural abundance, its biocompatibility, and its intrinsic properties combining high surface energy, semiconductivity and mechanical and chemical inertia, TiO_2 is one of the most attractive materials to be used in photocatalysis, self-cleaning optical coatings, solar energy conversion, energy storage, or sensing.[1] For such applications, TiO_2 required to be processed under homogeneous coatings of various thicknesses, while efficiency is directly proportional to the density of excitons created at the interface of the material. The efficiency becomes logically optimal when small anatase nanoparticles are arranged into a highly porous network to combine high surface area and high accessibility.[2] Constructing such highly porous nanocrystalline TiO_2 matrices have been, and is still, a priority in each one of these domains. Indeed, photocatalysis and dye sensitive solar cells requires several microns thick TiO_2 coating with high porosity, ideally composed of an assembly of hierarchical pores in the range of 2 to 50 nm to favour easy diffusion of pollutants or easy impregnation with the electrolytes, respectively.[3] Another important application concerns self-cleaning optical coatings, for which the thickness and the refractive index need to be accurately adjusted, through controlled processing conditions and porosity generation, to obtain the desired optical properties.[4] For instance, an anti-reflective self-cleaning [illegible] deposited on glass would require a refractive index arou[illegible] 1.25 in the visible range and a thickness close to 130 nm. If composed of anatase TiO_2 nanocrystals, it would combine antireflectivity, chemical durability and photo-induced self-cleaning. In parallel, the processing of these materials must be adapted to low-cost and rapid industrial production. In this respect liquid deposition techniques, such as dip coating or spray coating, followed by a fast thermal treatment would be preferred.[6] Many preparation routes to porous nanocrystalline TiO_2 coatings using liquid deposition have been reported.[7] They either involved preformed TiO_2 nanoparticles[7] or molecular precursors,[8] both combined with porogen organic agents such as block copolymers, surfactants, latex beads, or spinodal decomposition.[2] Most of these recipes are robust and lead to porous materials with different types of pore size distribution. However, they all reported relatively high refractive index and low porosity around 40% vol at maximum, which is due to intrinsic high refractive index of the bulk TiO_2 ($n \approx 2.5$ in the visible range) and the difficulty to prevent coating densification upon thermally induced crystallisation and diffusive sintering.[9] Low reflective, unique titanate or titania nanotube thin films were prepared by via layer-by-layer assembly;[10] while porosity of titanate films was evaluated being 64%, the refractive index remained quite high equal to 1.7. More recently, anatase aerogel films with porosity of 68% vol were achieved by supercritical drying however, this is a cumbersome methods that is not compatible with industrial production.[11] Another drawback associated to these thermal effects is the fragmentation of the layer above a typical thickness of 400nm that is created by the lateral tensile stress accompanying the network solidification. The denser the film is, the thinner is the cracking threshold. Cumbersome protocols, involving multilayer deposition accompanied by intermediate pre-stabilisation steps, are often proposed to overcome this problem and build up micron thick films.[12, 13]

[a] Sorbonne Universités, UPMC Univ Paris 06, CNRS, Collège de France, UMR 7574, Chimie de la Matière Condensée de Paris, F-75005, Paris, France.
[b] IM2NP, Faculté des Sciences et Techniques, Campus de Saint Jérôme, Avenue Escadrille Normandie Niemen, 13397 Marseille, France
david.grosso@upmc.fr

† Footnotes relating to the title and/or authors should appear here.
Electronic Supplementary Information (ESI) available

Here we report a simple, fast and low cost method to prepare ultra porous crystalline TiO_2 layer with thickness up to 1.5µm in a single step dip-coating process followed by a flash thermal treatment. We show that a combination of 3 different templating agents (PB-PEO, Pluronic F17, and PEG) with 10% SiO_2 in the solid composition allows not only to maintain a high porosity but also to prevent thick layer cracking upon thermal treatment without preventing the crystallisation of anatase nanoparticles. Exploiting the dip-coating method in the capillary regime,[14] we demonstrated that more than 1µm thick ultra-porous TiO_2-based films could be prepared in a single step. In addition the present material was used as negative resist for UV-lithography and as self-cleaning, antireflective coating. In order to achieve such a high porosity, several experiments were performed in which various solution compositions and processing conditions were combined. The experimental conditions and final refractive index of each studied combinations are reported in Table 1.

Table 1: Initial solution composition, thermal treatment conditions, and final refractive index measured by ellipsometry of films prepared on silicon wafers (ST-PBF* was deposited on glass. ST-PBF** was deposited on silicon wafer but underwent a slow thermal treatment). Ti5E corresponds to a stock solution that contains 1 $TiCl_4$ precursor for 5 EtOH solvent (molar ratio). TEOS stands for TetraEthylOrthoSilicate and F127, PEG6000 and PB-PEO are classical organic porogen templates (see the Notes section for further details).

Samples	*Ti5E*	*TEOS*	*F127*	*PEG6000*	*PB-PEO*	*Thermal curing*	n_{700nm}
ST-P	1.43g	0.08g	-	1.06g	-	5min 500°C	1.84
ST-F	1.43g	0.08g	1.06g	-	-	5min 500°C	1.33
ST-B	1.43g	0.08g	-	-	1.06g	5min 500°C	1.32
T-B	1.43g	-	-	-	1.06g	5min 500°C	1.44
ST-PBF	1.43g	0.08g	0.35g	0.35g	0.35g	5min 500°C	***1.27***
ST-PBF*	1.43g	0.08g	0.35g	0.35g	0.35g	5min 500°C	***1.35***
ST-PBF*	1.43g	0.08g	0.35g	0.35g	0.35g	10°C / min (500°C)	1.55

Initial solution compositions are listed in Table 1. For clarity purpose, the content in solvent is only reported in the Notes section. Sample T-B was prepared only for the purpose of direct comparison with ST-B. In the other cases, solutions composition were selected so that the total molar content in inorganic precursor and the total masse of porogen were kept constant at $x_{Ti} + x_{Si} = 3.8\ 10^{-3}$ mole and $m_{F127} + m_{PEG} + m_{PB\text{-}PEO} =$ 1.06 g, respectively. In the latter conditions, the theoretical porosity of the final layer that one would obtained after thermal transformation of precursors into dense SiO_2 and TiO_2 would be around 93% vol. This value is obtained through a simple calculation, assuming (i) the whole volume of organic phase to have transformed into void, (ii) no shrinkage of the porous network occurs, and (iii) approximating the initial component density to be $D_{SiO2} = 2$, $D_{TiO2} = 4$ and $D_{porogen} = 1$. According to the Bruggeman Effective Medium Approximation (BEMA) model,[15] the refractive index of such layers would then be 1.10, by assuming the reference refractive to be $n_{TiO2} = 2$ and $n_{SiO2} = 1.5$, respectively. In the present case, one observes in Table 1 that the refractive indexes are all measured by Ellipsometry to be above or equal to 1.27 at λ=700nm. Comparing first ST-P, ST-F and ST-B, for which only one type of porogen was used, one observes that the lowest refractive index is obtained for the PB-PEO and the F127 templates. This is due to the higher thermal stability of PB and PPO chains of both copolymers, compared to the PEG chains. Furthermore, PEG is known to, at least partially, interpenetrate the inorganic network while PB and PPO conform into micelle cores. The latter can thus withstand longer the thermal treatment, allowing thus a higher stiffening of the inorganic network, and consequently a lower shrinkage upon organic departure. This will be further discussed later in the article. Comparing the ST-B and T-B, in which the TEOS has been removed from the initial solution, reveals that the presence of 10% of silica intermediates into the inorganic network is beneficial to the preservation of the porosity. Very interestingly, the lowest refractive index of 1.27, corresponding to a porosity of 80 %vol, was only achieved for Sample ST-PBF, for which the three different templating agents were used in equal mass fraction. Finally, comparing the three ST-PBF samples, shows that such a high porosity is reduced either for a slower thermal treatment, or by changing the substrate from silicon wafer to conventional glass. The role of silica, of the substrate and of the thermal ramp will be discussed latter.

For the ST-PBF samples, to get from 93% theoretical porosity down to 80% deduced from the refractive index of 1.27, an unidirectional contraction of the global thickness of a factor of 2.8 must have occurred during the thermal treatment. In comparison, most reports on pure TiO_2 porous films give minimal refractive index barely above 1.6.[16] Figure 1 shows the SEM images of ST-PBF films made on Si wafers with 2 distinct thicknesses at 130 nm and 1500 nm and obtained in the draining and in the capillary regimes, respectively. They both exhibit similar structure characterised by a sponge-like, highly open and homogeneous porosity composed of interconnected pores of maximal dimension around 50 nm, as expected from the use of the present PB-PEO template.

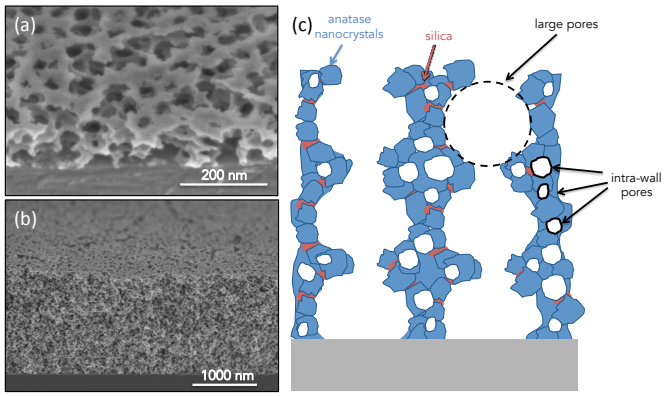

Figure 1 SEM images of a 130 nm thick (a) and a 1500 nm thick (b) ST-PBF films deposited on Si wafers and thermally treated at 500°C / 5min, and both having a refractive index of 1.27 at λ=700nm (measured by ellipsometry). (c) Schematic illustration of the hierarchical structure of the ultraporous TiO_2 based films .

The environmental ellipsometry porosimetry (EEP) analysis was then performed on the 130 nm thick film. The graph in Figure 2(a) represents the isotherm of adsorption/desorption of water plotted as the refractive index versus relative humidity. The adsorption curve progressively rises up to a refractive index value of 1.37 for a relative humidity very close to the saturation, before increasing suddenly to 1.63. The desorption branch shows a similar inversed tendency except that a hysteresis loop is observed between 0.95 and 0.75 P/P_0. These analysis reveals that the porosity is composed of around 75% vol. of large pores (clearly around a few tens of nm in dimension), clearly deduced from SEM investigation Figure 1, together with around 25% of a population of pores ranging from a few nm to the size of the large ones. This population will be addressed as intra-wall porosity from now. These pores of various dimensions are also observed from AFM investigation (see Figure S1), suggesting that all types of pores are found at the surface of the film. The GI-SAXS pattern of the ST-PBF sample is shown in Figure 2(b). The two symmetrical diffraction signals in the y direction close to the beam-stop, accompanied by the corresponding first harmonic at $2\pi/q$ = 28nm, corresponds to a periodic distance of 57 nm. This dimension is in agreement with the SEM and EEP results. The diffraction signals tend to extend in the z direction while becoming less intense, before they disappear totally behind the beam-stop, which is typical loss of ordering in directions normal to the surface. Such an effect has systematically been observed upon the thermal treatment and crystallisation of transition metal oxide mesoporous films that initially contained spherical template domains.[17]

The cristallinity of the TiO_2 framework is clearly evidenced by the GI-WAXS analysis shown in Figure S2 (right). The determination of the average size of the anatase nano crystals cannot be extracted from this analysis.[18] Because larger pores have lateral dimension of 50 nm while transversal periodicity was accurately measured at 57 nm by GI-SAXS, it is sensible to propose that walls thicknesses, and therefore anatase crystal dimension, are likely not to exceed 10 nm. This is confirmed by the HR-TEM micrograph of the system as shown in Figure S2 (right).

The role of the 10% silica is double. First, due to its low refractive index compare to that of TiO_2, it slightly reduces the refractive index of the inorganic phase. Second, its presence tends to increase the temperature of crystallisation of TiO_2 due to the stabilisation of the Ti species through the formation of Ti-O-Si oxo bonds at relatively low temperatures. It results in the formation of a high density of crystallisation nucleats under fast temperature raise, which then leads to small particles after growth. It is known that small particles are less stable than large ones and tends to grow by diffusive sintering at high temperature, provoking the collapsing of the pore network. However, in presence of a small amount of silica, we recently showed that for dense films, the growth of TiO_2 anatase nanoparticles by diffusive sintering is totally hindered even at 800°C.[19] The same effect is expected to be responsible for the low degree of shrinkage, and the maintaining of the high porosity, in the present case. Furthermore, the beneficial effect of the fast thermal treatment leading to n = 1.27 against 1.55 at 5°C/min, goes against what is generally observed for pure TiO_2 and other MO_n systems,[20] where a long and progressive thermal treatment is used to pre-stabilise the inorganic phase before crystallisation. With 10% SiO_2, a fast thermal treatment promotes the nucleation growth of anatase TiO_2 nanocrystals since a slow treatment will first induce the cross linking of the mixed amorphous network hindering the easy diffusion of Ti-oxo intermediate species. When the temperature at which one expects to see the crystallisation for pure TiO_2 is reached, the presence of stable Si-O-Ti bonds prevents easy diffusion of Ti-oxo species, favouring the local nucleation but reducing the growth. This effect that leads to the formation of well-dispersed embedded small nanocrystals has been well demonstrated for dense mixed silica-titania films. [19] As a result a fast thermal treatment is preferred in

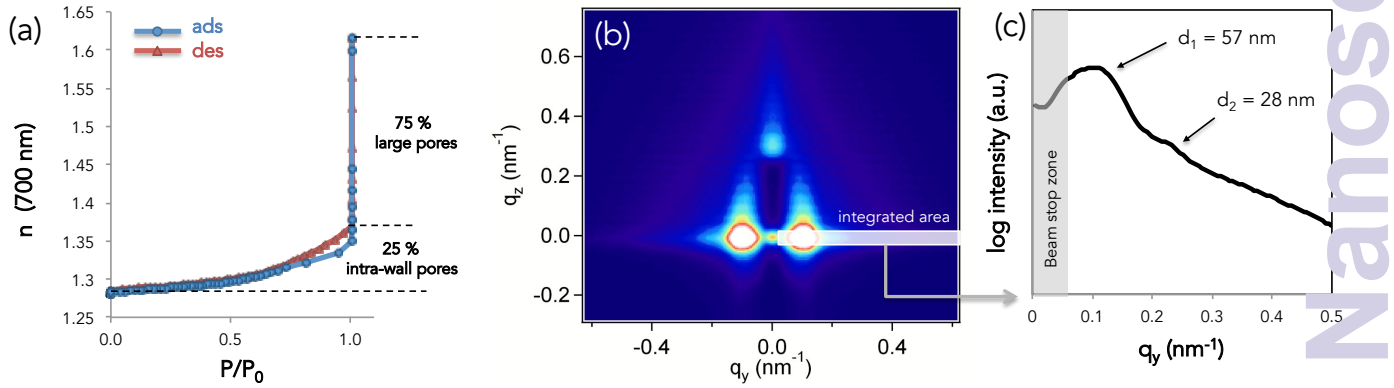

Figure 2 (a) Evolution of the refractive index of a 130 nm thick ST-PBF films, upon humidity increase (adsorption curve) and humidity decrease (desorption curve). Given percentages are calculated assuming a initial refractive index of 1.28 using the Bruggeman Effective Medium Approximation. (b) GI-SAXS 2D pattern and (c) the corresponding diagram of the intensity profile integrated on the dash white line of a ST-PBF typical film.

presence silica to preserve as much as possible the porosity. The high maintaining of a high porosity upon thermal treatment is not only attributed to the thermal treatment and the presence of SiO_2. Indeed, the type and the size of the porogen organic domains have also a key role. For instance, it is well known that "large" templating micelles form "large" pores and thick walls that can accommodate larger particles.[21] Both larger pores and larger particles present lower interface curvature that, according to the Laplace law, are more stable upon thermally induced diffusive sintering. This is verified here when comparing the refractive index of films prepared in exactly the same condition, except that the nature of the template was different for each case. The presence of PEG is known to lead to micropores[22] together with small mesopores, induced by microphase separation upon evaporation/condensation.[23] ST-P is thus expected to bear both micro and mesopores of various sizes. ST-F was prepared using only F127 template that leads to well defined 6-8 nm in diameter pores arranged into a bcc structure.[8] Larger pores of 50 nm in diameter are formed in the ST-B films for which a PB-b-PEO (22 000 – 15 500 $g.mol^{-1}$) template was utilised. As already stated, films are more porous when prepared with more thermally stable F127 or PB-b-PEO. Surprisingly, when mixing the three organic templates in equal mass proportion, we ended up with the lowest refractive index (n = 1.27) and therefore to the highest porosity (Sample ST-PBF), despite the presence of poorly stable PEG. As shown by the previous structural characterisation and as illustrated in Figure 1 (c), ST-PBF films are mainly composed of larges pores issued from PB-b-PEO, but 25% of the porosity are made of smaller pores, that are likely due to the use of F127 and PEG, and must to be. In view of the final porosity, one could imagine the three types of organic templates to have partially merged and self-organised during evaporation/condensation through an cooperative

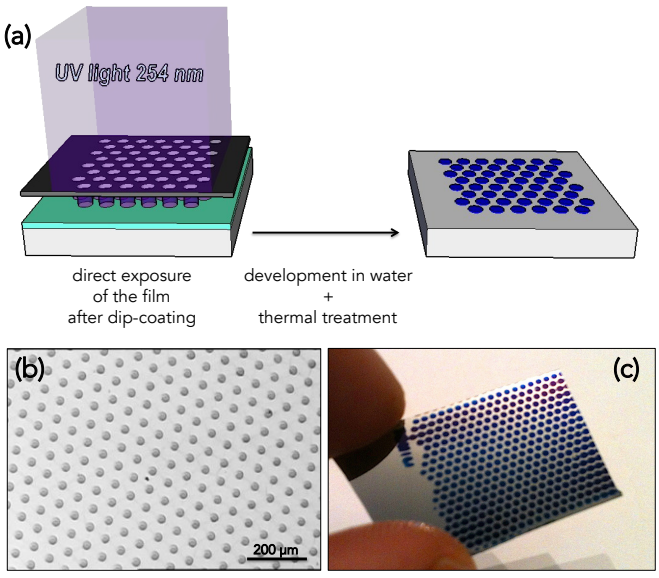

Figure 3 (a) Illustration of the patterning process by 254 nm UV lithography; (b) optical microscopy and (c) digital photographs of micrometric patterns of the ultraporous films.

mechanism involving quasi simultaneously the micellisation of F127, the co-packing of these with the already present in solution large PB-b-PEO micelles, together with the microphase separation of the PEG. Since, all three templates contain PEO chains, one expects them to intimately inter... more or less at the same time during the whole self-assembl... process. This is indeed a complex mechanism not ful... understood yet. A similar experiment was reported in ... previous paper in which titania films were templates by F12... and PPG leading to bimodal, larger pore's size network.[23] In that study, in similar conditions, the formation of very larg... pore was explained by the fact that some of the PPG molecules entered the micelles and acted as a pore swelling agent whi... the remaining PPG triggers demixing, originating the large mesopores. Upon flash thermal treatment, the hybrid system undergoes a rapid condensation of the inorganic species into a relatively stable network, accompanied by the therm... decomposition of the templates and the controlled diffusiv... crystallisation of anatase. Because the final porosity is mainl... composed of the large pores, one can state that the shrinkag... applied principally to the walls, where small pores with l... interface curvatures are located. The mechanical constraints created by the consolidation of the network are thus ma...., relaxed by the small pores collapsing. This leads to the thinning of the walls but not to the extended shrinkage of the glo... network. However, 25 % of the porosity is still composed b... small pores which is important since, as mentioned in th... introduction, efficiency of the layer is related to high surfac... area and thus to the presence of small pores. Finally, the fi... structure of the film has been represented in Figure 1B) where small residual nanopores of various dimensions can be found in the nano crystalline anatase walls of the larger mesopores. The 10% silica phase is likely to be located at the nanocrysta... boundary, but also agglomerated in between them. At least part of the anatase surface area is accessible to th... environment as deduced from the photocatalytic investigation (see further).

The ST-PBF as-prepared coating was also exploited as nega... resist for 254nm UV lithography. The patterning process is illustrated in Fig. 3a. After dip coating, the hybrid film is exposed to UV light (wavelength = 254nm) throug... micrometric stencil masks for 30 minutes. According to th... literature[24] and similarly to X-rays[25, 26], high energy ... radiation promotes the formation of free radicals H° and OH... from the residual water molecules present in the sol–gel film. Such radicals enhance the polycondensation kinetics of th... inorganic part and thus the consolidation by cross-linking o... the network. After UV exposure, the unexposed, uncondense... material is easily dissolved in water leaving the cross-linke... micrometric patterns. The final step is the thermal treatmen... at 500°C in order to yield the final materials with th... previously described characteristics. Figures 3 (b) and (c) shows two examples of hexagonally packed TiO_2 circular patches having diameters of 30 and 300 µm, respectively. It i... important to point out here that after UV exposure for 3... minutes and thermal treatment the resulting films exhi... refractive index of 1.27 (measured on a not-patterned sampl...

meaning that the patterning process does not affect the formation of the ultra-porous films. The micropatterning of such highly porous materials could open perspectives in several domains including: (i) macro- to microscale arrays (e.g., multiplexed or replicated structures and sensors) integrated in lab-on-a-chip devices or (ii) optical components such as diffraction gratings, mirrors or waveguides.

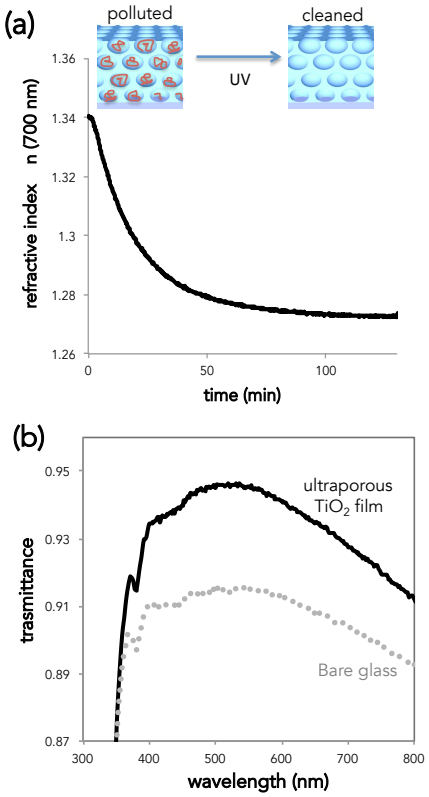

Figure 4 (a) Time evolution of the refractive index of a ST-PBF layer polluted with Lauric acid and submitted to UV irradiation. (b) UV-Visible transmittance spectra of a microscope glass slide substrate before and after deposition of a ST-PBF layer with 130 nm thickness and 1.35 refractive index.

As mentioned previously, these highly porous TiO_2 based films systems may be of great interest for applications requiring photoactive layers. One of the most important concerns antireflective self-cleaning coatings for solar panels for instance. Indeed, a TiO_2 antireflective coating would ensure perfect maintaining of the optical properties upon constant degradation of the organic pollutants getting in contact with the layer surface and porosity. Self-cleaning and the antireflective properties were investigated using UV-visible spectroscopy and ellipsometry. Results are provided in Figure 4 (a) and (b) respectively. In Figure 4 (a), the refractive index of a 130 nm thick ST-PBF film, artificially polluted with Lauric acid, was recorded during irradiation at 365nm. The initial refractive index of the empty film was 1.27 and was increased up to 1.34 after pollution, suggesting that part of the porosity is homogeneously filled up with Lauric acid. Upon irradiation, the refractive index clearly regained its initial value of 1.27 after around 1h, confirming the efficient photoactivity of the layer. The presence of 10% SiO_2 within the network does not hinder the formation of radical species and their activities as already demonstrated for nanocomposite SiO_2/TiO_2 materials[27] and other systems.[28]

The ST-PBF** sample is composed of the same ST-PBF laye but deposited on glass side (one side coated). On suc substrate the refractive index of the layer was measured to b 1.35 and not 1.27 as it was found with Si substrates. Th difference may be attributed to the difference in heat transfer during flash treatment. Indeed, glass has a much low thermal conductivity than Si, which could sufficiently slow down the heating of the film itself and provokes a greate network contraction. A second possible reason for the lower refractive index of the ST-PBF** is ionic diffusion of from the glass substrate into the TiO_2 layer that induces easier contraction of shrinkage of the network and optical inde increase.[29] Even if both these effects can be avoided (b speeding up the flash treatment on glass for the first one, an by intercalating a dense and pure silica sol-gel *buffer* laye between the substrate and the AR coating), an efficient coating needs also to be mechanically robust. Therefore, an AR coating with a higher refractive index will always be m robust than with a lower one. Here, the ST-PBF** film is still antireflective with a refractive index of 1.35, since between and 4% transmittance was gained all over the solar emissio spectrum, when compared to bare glass, as shown in Figur 4(b).

The ST-PBF films were proved to be superhydrophilic sinc nearly 0° contact angle was measured by contact angle analysis (reported in S3). This property can be ascribed to th combined effects of chemical composition and mesostructure: (i) the intrinsic chemical nature of TiO_2 whose hydrophobici is enhanced when exposed to UV radiation[30] and (ii) the presence of an interconnected porous network that enable porous wicking by capillarity.[31] The superhydrophilicity of the layer is well known to confer anti-fogging properties to th surface. By inducing complete wetting of water on the surface, condensed water forms a thin sheet of water, rather th individual sessile droplets, reducing random scattering o light.[30] Concerning mechanical stability, the ST-PBF and ST-PBF** films are highly porous and are thus expected to b relatively fragile. However, they have been cleaned wit water, acetone and ethanol without modifying their op properties. Only a relatively strong and repetitive han cleaning with a water soak tissue for several minutes provoke the alteration of the optical properties for the more porous ST PBF sample on Si. Finally, we also showed that making ultr thick layers of this ultra-porous TiO_2 is possible through dip coating in capillary regimes (see Figure 1b), which could b extremely useful in photocatalysis and for Dye Sensitized Sola Cells. In particular, the extinction coefficient at λ = 350 nm wa 0.05 (by ellipsometry). This relatively low value is attributed t the high porous volume of the film. Very efficient U photoactivation is thus expected for ultra-thick layers since the penetration depth at 350 nm was evaluated being equal to 55 nm.

Conclusions

We demonstrated that 90% rich anatase TiO_2 based mesoporous films with thickness up to 1.5 µm and refractive index down to 1.27 (high porosity up to 80% vol) can be prepared in a single layer deposition by dip-coating a solution composed of $TiCl_4$ precursor and a mixture of 3 different hierarchical PEO-based organic templates. The films are crack-free and of optical quality. The method has been demonstrated on two different substrates (Si and glass) and can potentially be scaled-up to large surfaces by exploiting a recently reported "bi-phasic" dip-coating method.[32] The stability of the films toward thermal treatment induced internal stresses, that are usually responsible for the porosity collapsing and the formation of lateral cracks, has been attributed to the combined effect of the 10% SiO_2 content, a rapid thermal treatment, and the existence of pores with various sizes and interfacial curvatures allowing the efficient relaxation of the interfacial strength. The intrinsic photocatalytic activity of the films was evidenced by totally cleaning the porous network from organic pollutants upon 1h UV irradiation. The versatility of the presented system was demonstrated by exploiting it as UV-lithography resist and anti-reflective, self-cleaning, superhydrophilic coating. The hierarchical characteristic of the porosity, together with the high porosity, makes these layers serious candidates to be used as active components in Dye sensitive Solar Cell, antireflective self-cleaning optical coating, photocatalysis, sensors, or biocompatible layer for implant compatibilisation.

Notes and references

Initial solutions were prepared using absolute EtOH, TetraHydroFurane (THF), deionised H_2O, PolyEthylene Glycol (PEG 6000), (EO)106(PO)70(EO)106 (Pluronic F127) and PB-b-PEO (22 000 – 15 500 $g.mol^{-1}$) block copolymers, TetraEthylOrthoSilicate (TEOS) and $TiCl_4$ chemicals. A first solution composed of 1 $TiCl_4$ for 5 EtOH, named Ti5E, is prepared by gently adding $TiCl_4$ in cooled EtOH (care must be taken since this is a highly exothermic reaction). The organic agents were then dissolved in 31g EtOH + 3g H_2O for samples that did not contain PB-b-PEO and 26g EtOH + 0.75g H2O + 6g THF for samples that contained PB-b-PEO. Finally, Ti5E and TEOS were added into the solution in the proportions listed in Table 1. The solutions were then allowed to age between 1h and several days before been used for coating processing (no effect of the ageing time on the film properties was observed). Silicon wafer or microscope glass slides substrates were used as substrates. They were cleaned in acetone before been coated. Coatings were performed by dip-coating in the Landau Levitch regime at room temperature and ambient humidity using a withdrawal speed of $3mm.s^{-1}$. Thick films were also prepared by dip-coating but in the capillary regime at 0.01 mms^{-1} As prepared films were then placed under a hot IR lamp and were then allowed to be cured at 500°C for 5 min or up to 500°C with a heating ramp of 10°C.min-1. The ST-PBF** film was deposited on microscope glass slides. Only one face was coated since the second one was cleaned up with a tissue soak with ethanol before thermal treatment. The patterning of the films was obtained by exposing the as dipped hybrid films to a UV radiation trough stencil masks. The sample was then placed at 1cm under a UV-lamp (254 nm / 0.48 $mW.cm^{-2}$) for 30 minutes. After exposure the sample was gently rinsed in water in order to dissolve the uncondensed materials. The Field Emission Gun Scanning Electron Microscopies were obtained using a SEM-FEG Zeiss Ultra 55. X-ray analyses were performed by Grazing Incidence Small-Angle X-ray Scattering (GI-SAXS-Rigaku S-max 3000 equipped with a microfocus source λ=0.154nm and a 2D Gabriel type detector place at 1480 mm from the sample (all under vacuum), at an incident angle of 0.21°; the direct and specular reflected beams were masked by a vertical beam-stop), and Wide Angle X-ray Diffraction (GI-WAXS: same set up as GI-SAXS except that diagrams were obtained by radial integration of the signal obtained on a image plate placed at 5 cm from the sample centre). Ellipsometry measurements were performed on a UV-visible (from 350 to 1000 nm) variable angle spectroscopic ellipsometer (VASE – 2000U Woollam), and the data analyses were performed with the Wvase32 software using the Cauchy model. Environmental Ellipsometry Porosimetry was investigated through capillary condensation of water into the porosity using an atmospheric control chamber and using the Bruggeman Effective Medium approximation. Photoactivity of the systems was investigated by following the refractive index of the layer, contaminated with Lauric acid, upon UV irradiation. Lauric Acid (LA) was selected because it has already been studied as model pollutant at TiO_2 interfaces under UV and because it's physical-chemical properties (poor volatility) make simple its homogeneous infiltration and stabilisation within mesoporous films.[33] The porosity was thus previously filled with Lauric acid by liquid deposition from a concentrated solution in ethanol. The filling fraction was evaluated by BEMA model being equal to 50% of the porosity as reported in S4. The polluted sample was then placed at 3cm under a UV-lamp (365 nm / 0.48 $mW.cm^{-2}$) and optical density was recorded every minute using the previous ellipsometry conditions over a period of 3 days. The UV/Vis absorption spectra were recorded by using a UVIKON XL-SECOMAM (UVK-Lab) spectrometer directly on the one side coated glass samples. The background was recorded in air only.

1. X. Chen and S. S. Mao, *Chemical Reviews*, 2007, 107, 2891-2959.
2. D. Fattakhova-Rohlfing, A. Zaleska and T. Bein, *Chemical Reviews*, 2014, 114, 9487-9558.
3. M. Pagliaro, G. Palmisano, R. Ciriminna and V. Loddo, *Energy & Environmental Science*, 2009, 2, 838-844.
4. C. Euvananont, C. Junin, K. Inpor, P. Limthongkul and C. Thanachayanont, *Ceramics International*, 2008, 34, 1067-1071.
5. H. K. Raut, V. A. Ganesh, A. S. Nair and S. Ramakrishna, *Energy & Environmental Science*, 2011, 4, 3779-3804.
6. M. Faustini, C. Boissière, L. Nicole and D. Grosso, *Chemistry of Materials*, 2013, DOI: 10.1021/cm402132y.
7. T. Brezesinski, J. Wang, J. Polleux, B. Dunn and S. H. Tolbert, *Journal of the American Chemical Society*, 2009, 131, 1802-1809.
8. E. L. Crepaldi, G. J. d. A. A. Soler-Illia, D. Grosso, F. Cagnol, F. Ribot and C. Sanchez, *Journal of the American Chemical Society*, 2003, 125, 9770-9786.
9. D. Grosso, G. J. d. A. A. Soler-Illia, E. L. Crepaldi, F. Cagnol, C. Sinturel, A. Bourgeois, A. Brunet-Bruneau, H. Amenitsch, P. A. Albouy and C. Sanchez, *Chemistry of Materials*, 2003, 15, 4562-4570.
10. M. Miyauchi and H. Tokudome, *Thin Solid Films*, 2006, 515, 2091-2096.
11. W. Sung, S.-H. Hyun, D.-H. Kim, D.-S. Kim and J. Ryu, *J Mater Sci*, 2009, 44, 3997-4002.

12. J. Dewalque, R. Cloots, F. Mathis, O. Dubreuil, N. Krins and C. Henrist, *Journal of Materials Chemistry*, 2011, 21, 7356-7363.
13. N. Krins, M. Faustini, B. Louis and D. Grosso, *Chemistry of Materials*, 2010, 22, 6218-6220.
14. M. Faustini, B. Louis, P. A. Albouy, M. Kuemmel and D. Grosso, *Journal of Physical Chemistry C*, 2010, 114, 7637-7645.
15. C. Boissiere, D. Grosso, S. Lepoutre, L. Nicole, A. B. Bruneau and C. Sanchez, *Langmuir*, 2005, 21, 12362-12371.
16. G. J. A. A. Soler-Illia, P. C. Angelome, M. C. Fuertes, D. Grosso and C. Boissiere, *Nanoscale*, 2012, 4, 2549-2566.
17. D. Grosso, F. Cagnol, G. J. d. A. A. Soler-Illia, E. L. Crepaldi, H. Amenitsch, A. Brunet-Bruneau, A. Bourgeois and C. Sanchez, *Advanced Functional Materials*, 2004, 14, 309-322.
18. M. Faustini, L. Nicole, C. Boissière, P. Innocenzi, C. Sanchez and D. Grosso, *Chemistry of Materials*, 2010, 22, 4406-4413.
19. B. Louis, N. Krins, M. Faustini and D. Grosso, *The Journal of Physical Chemistry C*, 2011, 115, 3115-3122.
20. C. Sanchez, C. Boissière, D. Grosso, C. Laberty and L. Nicole, *Chemistry of Materials*, 2008, 20, 682-737.
21. X. Jiang, N. Suzuki, B. P. Bastakoti, W.-J. Chen, Y.-T. Huang and Y. Yamauchi, *European Journal of Inorganic Chemistry*, 2013, 2013, 3286-3291.
22. J. M. Calderon-Moreno, S. Preda, L. Predoana, M. Zaharescu, M. Anastasescu, M. Nicolescu, M. Stoica, H. Stroescu, M. Gartner, O. Buiu, M. Mihaila and B. Serban, *Ceramics International*, 2014, 40, 2209-2220.
23. L. Malfatti, M. G. Bellino, P. Innocenzi and G. J. A. A. Soler-Illia, *Chemistry of Materials*, 2009, 21, 2763-2769.
24. L. Brigo, G. Grenci, A. Carpentiero, A. Pistore, M. Tormen, M. Guglielmi and G. Brusatin, *J Sol-Gel Sci Technol*, 2011, 60, 400-407.
25. M. Faustini, B. Marmiroli, L. Malfatti, B. Louis, N. Krins, P. Falcaro, G. Grenci, C. Laberty-Robert, H. Amenitsch, P. Innocenzi and D. Grosso, *Journal of Materials Chemistry*, 2011, 21, 3597-3603.
26. P. Falcaro, L. Malfatti, L. Vaccari, H. Amenitsch, B. Marmiroli, G. Grenci and P. Innocenzi, *Advanced Materials*, 2009, 21, 4932-+.
27. W. Dong, Y. Sun, C. W. Lee, W. Hua, X. Lu, Y. Shi, S. Zhang, J. Chen and D. Zhao, *Journal of the American Chemical Society*, 2007, 129, 13894-13904.
28. M. Gohin, E. Allain, N. Chemin, I. Maurin, T. Gacoin and J.-P. Boilot, *Journal of Photochemistry and Photobiology A: Chemistry*, 2010, 216, 142-148.
29. B. E. Yoldas, *Applied Optics*, 1982, 21, 2960-2964.
30. R. Wang, K. Hashimoto, A. Fujishima, M. Chikuni, E. Kojima, A. Kitamura, M. Shimohigoshi and T. Watanabe, *Nature*, 1997, 388, 431-432.
31. J. Bico, C. Tordeux and D. Quéré, *EPL (Europhysics Letters)*, 2001, 55, 214.
32. D. R. Ceratti, B. Louis, X. Paquez, M. Faustini and D. Grosso, *Adv. Mater.*, 2015, 27, 4958.
33. R. Li, M. Faustini, C. Boissiere and D. Grosso, *Journal of Physical Chemistry C*, 2014, 118, 17710-17716.